PERGAMON

International Journal of Solids and Structures 38 (2001) 2517–2532

INTERNATIONAL JOURNAL OF SOLIDS and STRUCTURES

www.elsevier.com/locate/ijsolstr

On crack-tip cooling during dynamic crack initiation

O. Bougaut [1], D. Rittel *

Faculty of Mechanical Engineering, Israel Institute of Technology, Technion city, 32000 Haifa, Israel

Received 1 July 1999; in revised form 19 April 2000

This paper is dedicated to Prof. Dietmar Gross on the occasion of his 60th birthday.

Abstract

This paper presents a hybrid experimental–numerical treatment of the transient thermoelastic effects around a crack tip, subjected to a dynamic loading. A simple numerical procedure was devised to calculate the transient crack-tip temperature field, in a ''one-way'' coupled approach. The calculations were carried out in two steps: first the evolution of the volumetric strain is determined by solving the mechanical problem. Next, this strain is converted into a nodal heat generation rate to solve the associated thermal problem for the same geometry. This approach was validated through the comparison of simulated and experimentally determined crack-tip temperatures. The experiments were carried out on instrumented compact compression PMMA specimens. These numerical results confirm and extend previous results concerning crack-tip cooling effects (Rittel, D., 1998a. In: Durban, D., Pearson, J.R.A. (Eds.), IUTAM Symposium on Non-linear Singularities in Deformation and Flow. Kluwer Academic Publishers, Dordrecht, pp. 181–192; Rittel, D., 1998b. Int. J. Solids and Structures 35 (22), 2959–2973). They show the three-dimensional nature of the thermal field, with increased cooling effects at specimen's mid-thickness. The present results also confirm that adiabatic conditions prevail during the initial stages of the dynamic fracture process. Finally, it is shown that the crack-tip cooling effect characterizes the response of linear thermoelastic materials, regardless of their thermal conductivity. © 2001 Published by Elsevier Science Ltd.

Keywords: Thermoelastic; Impact; Dynamic fracture; Polymers; Cooling; Adiabaticity

1. Introduction

It is a well established fact that thermomechanical couplings play an important role in fracture. Many studies have been devoted to the investigation of temperature changes ahead of propagating cracks in various types of solids, with emphasis on crack propagation stages and associated temperature rise. Weichert and Schönert (1978) investigated dynamic crack propagation, both theoretically and experimentally. Using infrared detection technique, these authors showed a significant temperature rise associated with the crack propagation in glass. In this same work, a noticeable temperature drop is reported prior to the onset of propagation. Several authors have shown that transient (mode I) loading of a thermoelastic

* Corresponding author. Tel.: +972-4-829-3261; fax: +972-4-832-4533.
E-mail address: merittel@tx.technion.ac.il (D. Rittel).
[1] Permanent address: Ecole Polytechnique, 91128 Palaiseau Cedex, France.

0020-7683/01/$ - see front matter © 2001 Published by Elsevier Science Ltd.
PII: S0020-7683(00)00168-2

material induces crack-tip cooling (Fuller et al., 1975; Sih and Tzou, 1986; Rittel, 1998a,b). Crack-tip cooling is also mentioned in the numerical study of Sun and Hsu (1996). Analytical solutions of various thermomechanically coupled fracture problems have been proposed by Brock (1996, 1999a), including the possibility of crack-tip cooling (Brock, 1999b). While this literature survey is far from being exhaustive, it, nevertheless, indicates that stress-induced dilatancy ahead of the crack-tip induces a transient cooling effect, whose magnitude is not necessarily negligible. Recently, Rittel (1998b) investigated the thermoelastic effect in a stress wave loaded brittle polymer polymethylmethacrylate (PMMA), using small embedded thermocouples. One result was that fracture initiates during the cooling phase. Simple estimates of the temperature drop ahead of the crack-tip were based on assumptions of linear elastic fracture mechanics, and adiabaticity. It was assumed that the temperature drop exhibits a $r^{-1/2}$ singularity. The embedded thermocouple technique provided a point indication of the temperature drop at a fixed location which includes the thermal history, *prior to* and *during* crack propagation. In a previous work, Rittel (1998a) suggested that crack-tip cooling was not restricted to poor thermal conductors, such as polymers, and it should apply to other materials as well, provided a dominant (thermo)elastic response. This suggestion was based on a simple analytical solution of the problem in which adiabatic conditions were assumed to prevail during fracture.

In this paper, we address additional aspects of the thermoelastic coupling by combining numerical (coupled) thermoelastic simulations and experimental work. Adiabatic conditions are *not* assumed here. The numerical simulations provide estimates of the temperature field, in which measurements are made at a particular point (similar to an embedded thermocouple). The agreement between numerical and experimental results validates the numerical model. The validation opens the way for additional purely "numerical experiments". Two specific issues are thus addressed. The first concerns the *validity of the assumptions* of adiabaticity during the initial stages of dynamic crack initiation. The second question concerns the extent to which *thermal conductivity* affects the transient crack-tip thermal effects.

The paper is organized as follows: Section 2 briefly reviews the experimental aspects of this work. Section 3 details the numerical method for thermoelastically coupled finite element calculations. Section 4 introduces the procedure used to extrapolate the temperature at any point located along the crack line and through the specimen thickness. In the same section, we simulate the evolution of the temperature, as sensed by the stationary (numerical) thermocouple. In Section 5, we compare and discuss experimental and numerical results. Section 6 introduces additional numerical results about adiabaticity and the influence of the thermal conductivity of the material. Section 7 summarizes and concludes this work.

2. Experimental

The goal of the experiment is to measure simultaneously the applied forces, fracture time and crack-tip temperature. The experimental setup and the instrumentation of the specimen, shown in Fig. 1, will be briefly described. A full account of the experimental procedure can be found in Rittel (1998b).

2.1. Material

We used commercial PMMA as a model brittle material. The various properties of PMMA, which are listed in Table 1, were determined by Rittel and Maigre (1996).

2.2. Specimen

The dynamic fracture experiments were carried out on compact compression specimens (CCS). The geometry of this specimen causes crack opening under compressive loads (Rittel et al., 1992). Maigre and

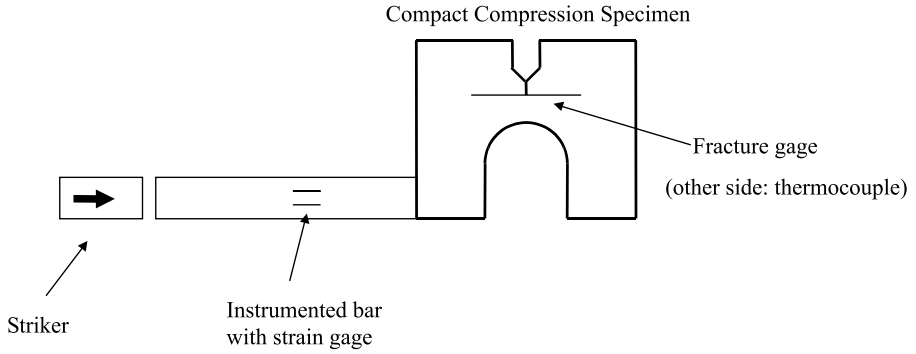

Fig. 1. The experimental setup: An instrumented bar is brought in contact with a CCS. The latter is instrumented at its mid-thickness with an embedded thermocouple, and on its surface by a single wire fracture gage.

Table 1
PMMA and steel properties determined after Tadmor (1979) and Holman (1986), respectively

	PMMA	Steel
Dynamic Young's modulus (Pa)	5×10^9	2.1×10^{11}
Poisson's ratio	0.37	0.3
Density (kg/m^3)	1180	7800
Longitudinal wave velocity (m/s)	1200	5100
Thermal conductivity (W/m K)	0.2	54
Glass transition temperature (K)	373	None
Specific heat (J/kg K)	1200	465
Dynamic fracture toughness (MPa m$^{1/2}$)	5	50

Rittel (1993) showed that, for this specimen, mixed mode fracture occurs, with a dominant mode I component. The thickness of the specimen was 11.4 mm. The initial notch was extended by careful fatigue precracking. The CCS was instrumented with a silk-screened single wire fracture gage (silver conductive paint), located at about 1 mm from the crack tip. Opposite to this gage, a 0.3 mm diameter hole was drilled through mid-thickness of the specimen. A small K-type (copper-constantan) thermocouple was then inserted and sealed, using home-made liquid PMMA. A detailed description of the embedded thermocouple technique can be found in Rittel (1998c) and Rabin and Rittel (1999).

2.3. Stress wave loading apparatus (Rittel, 1998b)

An instrumented (strain gage) 12.5 mm diameter steel bar was used to apply and measure transient loads. The specimen lies unsupported and is in contact with one extremity of the bar. As a steel cylindrical striker is fired against the other end of the bar, a compressive (incident) pulse propagates towards the specimen. Part of the stress wave (reflected) reflects at the specimen–bar interface. The resulting interfacial force and velocity are determined from the incident and reflected signals, after their correction for geometrical dispersion and attenuation. The single-wire fracture gage signals the onset of crack propagation. All signals (strain gage, fracture gage, thermocouple) were simultaneously recorded using a Nicollet 490 digital oscilloscope. It should be noted that fracture occurs by inertia only, as in previous similar experiments.

3. Numerical modeling

A two-dimensional, plane strain, dynamic analysis of the CCS was carried out, using ANSYS (1994) commercial finite element package. We assumed a linear elastic material behavior. The crack was treated as stationary, to simulate the specimen prior to crack propagation (Rittel, 1998b). The fully coupled problem requires the simultaneous solution of the mechanical and the thermal problem. This procedure involves complex algorithms (Sun and Hsu, 1996). We adopted a simpler procedure, in which the mechanical to thermal energy conversion (thermomechanical coupling) was treated sequentially. The two consecutive steps of this "one-way-coupled analysis", are shown in Sections 3.1 and 3.2.

3.1. First step: mechanical analysis

The first step consists of solving the equation of motion for the cracked specimen:

$$\nabla \cdot \sigma = \rho \ddot{u}, \tag{1}$$

where σ is the stress tensor and u represents the displacement vector (superposed dots indicate time derivatives) and ρ is the material's density. The specimen (CCS) lays unsupported and is initially at rest: $u(t=0)=0;\ \dot{u}(t=0)=0;\ \ddot{u}(t=0)=0$. The force $F(t)$ is applied to the part of the CCS which is in contact with the input loading bar (Fig. 1).

The CCS was discretized into triangular and quadrilateral (1737) finite elements (PLANE 42). The crack-tip was modeled with quarter-point singular triangular elements (Barsoum, 1978). The applied force was modeled as a pressure applied to the structure. This parameter could either be determined experimentally (for a subsequent hybrid experimental-numerical approach), or arbitrarily selected (for numerical experiment). The equation of motion were solved, using Newmark time integration scheme (Bathe, 1982). At each time step i, the volumetric strain increment $\dot{\varepsilon}^i_{kk}$ was calculated and stored for each node n, according to $\dot{\varepsilon}^i_{kk} = [\varepsilon^{i+1}_{kk} - \varepsilon^i_{kk}]/\Delta t$, where $\Delta t = 1$ μs (time step).

The mode I and mode II stress intensity factors were calculated from the opening and shear crack opening displacements, as in Bui et al. (1992).

3.2. Second step: thermal analysis

Following Boley and Weiner (1960), when inelastic deformations are neglected, the coupled heat equation is written as

$$k\nabla^2 T - \alpha T_0(3\lambda + 2\mu)\dot{\varepsilon}^{\mathrm{e}}_{kk} = \rho c \dot{T}, \tag{2}$$

where T is the temperature (T_0: reference), α is the thermal expansion coefficient, λ and μ stand for Lamé constants. The superimposed dot indicates time derivative and the summation convention is assumed. In this equation, internal heat generation is caused by elastic dilatation, according to

$$Q = \alpha T_0(3\lambda + 2\mu)\dot{\varepsilon}^{\mathrm{e}}_{kk}.$$

The volumetric heat generation rate at each step term Q^i_n was thus calculated from the previously determined $\dot{\varepsilon}^i_{kk}$.

Therefore, upon completion of the first step, the element type was switched to *thermal* (PLANE 55) in order to solve Eq. (2). The initial temperature was assumed to be uniform, and equal to 293 K. The prescribed nodal heat generation rate was set to Q^i_n at each time step. Thermal convection was prescribed on the boundaries of the specimen and along the crack flanks. A value of 15 W/m^2 K for the thermal convection coefficient was assumed. The transient heat equation (Eq. (2)) was then solved at each time step,

yielding the *temperature field* in the specimen. The additional thermal properties are given in Table 1. Note that adiabaticity was not assumed a priori.

4. Processing of the thermal data

The numerical analysis provides the 2D temperature field for each node at each time step. Procedures are described next to obtain a *continuous* spatial thermal field, with a discrete temporal evolution.

4.1. Temperature as a function of the distance to the crack tip

The origin of the coordinates is located at the tip of the crack. The simulation gives the temperature of n aligned nodes, along a radius vector r at a given angle Θ. The temperature around the crack tip, at any distance r from the crack tip, is assumed to be given by $T(r) = \alpha/\sqrt{r}$, where α is a real coefficient. Coefficient $\alpha(t)$ is determined by a least square minimization at each time step:

$$\alpha = -\frac{\sum_{i=1}^{n} \hat{T}(x_i) \Big/ \sqrt{x_i}}{\sum_{i=1}^{n} 1/x_i}, \tag{3}$$

where $\hat{T}(x_i)$ is the temperature at point number i. In the following calculations, four nodes were selected at $\Theta = 0$. The assumption of a singular temperature field is not based on physical evidence. This assumption is made to match LEFM predictions. A more physical situation is that of a finite crack-tip temperature, by analogy with finite crack-tip deformations and stresses.

4.2. Temperature as a function of the thickness of the specimen

Points located at mid-thickness of the specimen deform under plane strain. By contrast, surface points are subjected to a plane stress state. These two problems were simulated. We then assumed that the distribution of the temperature is a linear function of the thickness. This is, of course, a first assumption, until a fully coupled 3D solution is obtained.

4.3. Simulation of the thermocouple recording

The experiment provides three results: the applied force, the fracture time, and the thermocouple's reading. The force is used as a boundary condition. The calculated and the measured temperatures can be compared to validate the numerical procedure. As the thermocouple stands along the crack path, it records the information from both the stationary and the propagating crack until its destruction (Rittel, 1998b). To simulate the reading of the thermocouple, we assumed that the crack is stationary until a time t_f, and it subsequently propagates at constant velocity v. Let $d(t)$ be the distance between the crack tip and the thermocouple at time t, with $d(t = t_f) = D$.

At $t \leqslant t_f$ (fracture time): The crack is stationary, $d(t) = D$, thus $T(t) = \alpha(t)/\sqrt{D}$. Eq. (3) was used for the calculation of $\alpha(t)$.

At $t > t_f$: The crack "propagates" at velocity v, therefore $d(t) = D - v(t - t_f)$ and $T(t) = \alpha(t)/\sqrt{D - v(t - t_f)}$.

This procedure comprises two degrees of freedom. The first is the crack velocity, v. The second is the fracture time. The actual fracture time precedes that indicated by the fracture gage by about 10 μs, needed for the microcracks to initiate at mid-thickness, coalesce, reach and destroy the surface wire gage (Maigre and Rittel, 1996; Rittel and Maigre, 1996; Rittel, 1998b).

At this stage, it should be emphasized, to avoid any confusion, that the crack tip does not actually propagate in the numerical experiments. The propagation effect is achieved by letting the distance between the crack tip and the virtual thermocouple diminish.

5. Experimental results and their simulation

5.1. Stress intensity factors

Fig. 2 shows the calculated evolutions of the stress intensity factors for a typical fracture experiment (PMMA102). The origin of time is taken as the time at which the specimen-bar interface is loaded. The signals remain almost constant for the first 30 μs, until the crack is loaded. Thereafter, the crack-tip experiences mixed-mode loading with a dominant mode I component, beyond 50 μs. In this experiment, the fracture gage indicated fracture at $t_f = 56$ μs.

5.2. Calculated temperature

Fig. 3 shows the calculated temperature ahead of the crack tip, for this experiment, at various distances ($\theta = 0°$, 230, 380, 500, and 620 μm). Until 40 μs, there is no noticeable temperature change. The temper-

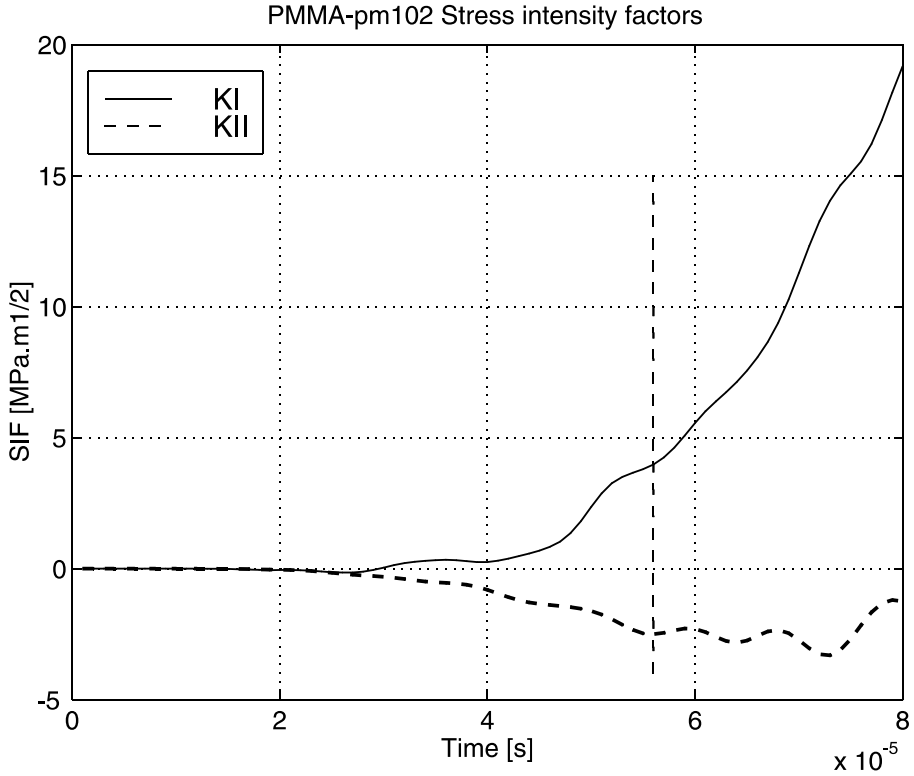

Fig. 2. Calculated stress intensity factors for a typical experiment (pm102). Note the dominance of mode I. Fracture was detected at 56 μs, as indicated by the vertical dashed line.

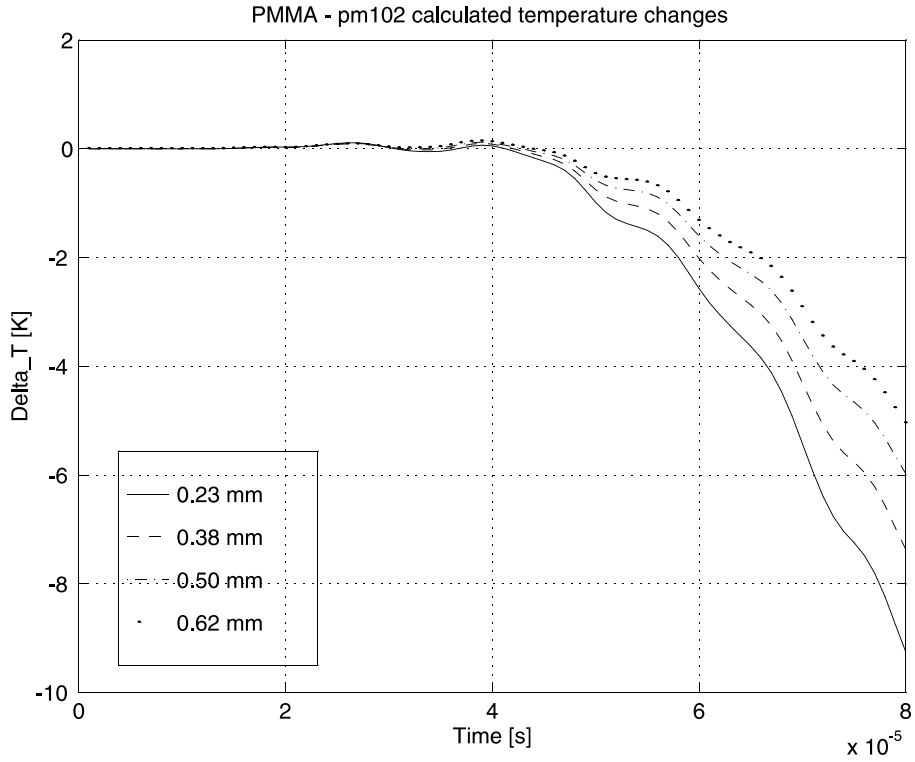

Fig. 3. Calculated temperature drop ahead of the crack-tip for the same experiment. The temperature drop is more severe as the distance to the crack tip decreases.

ature starts to decrease thereafter, reaching about $\Delta T = 2$ K at fracture, at a minimum distance of 230 μm from the crack tip at fracture time. This result is in agreement with the stress intensity factor K_I, which becomes markedly positive after 30 μs. From this figure, it can be noted that the cooling effect is increasingly evident as the distance from the crack tip decreases. The radius of the plastic zone size at fracture is of the order of 4.3 μm, for $K_I = 4$ MPa $m^{1/2}$, $\sigma_{yd} = 200$ MPa and $v = 0.37$, (Rittel, 1998b). Eq. (2) can be used to extrapolate the temperature, closer to the stationary crack-tip, as shown in Fig. 4. Here, the temperature drop reaches about $\Delta T = 8$ K, at fracture time, at a distance roughly equal to five plastic zone radii (20 μm).

5.3. Comparison of experimental and numerical results

Further insight is gained by comparing the measured temperature record with a numerical simulation. The parameters of the simulation are, according to Section 4.3, the fracture time t_f, crack velocity v, and initial distance between the crack-tip and the thermocouple D (see Eq. (3)). The fracture time cannot be assessed precisely from fracture gage indications, since the latter indicates *completion of the process*. Therefore, the *onset of fracture* is assumed to start before the fracture time indicated by the fracture gage. The (constant) crack velocity is not measured in the present experiments and its value has to be assumed. Finally, the accurate value of D is difficult to assess because of the crack-front curvature, with respect to the embedded thermocouple. Therefore, all three parameters are subjected to uncertainty. However, it was observed that they must not be *uniquely* determined to get a physically realistic simulation of the

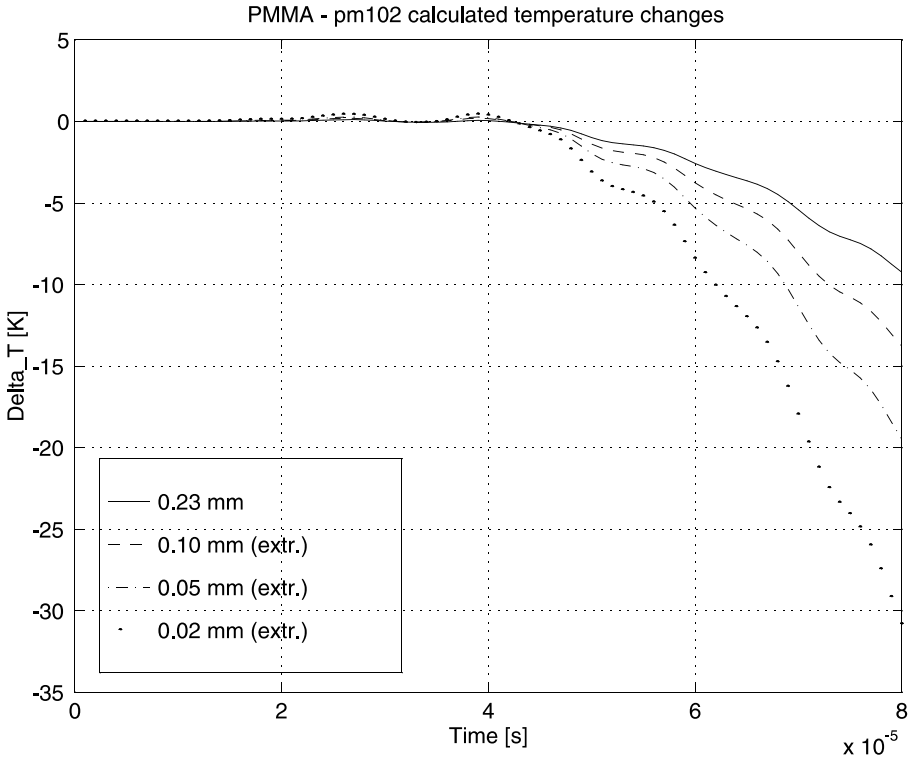

Fig. 4. Extrapolated temperature drop ahead of the crack tip for the same experiment. The distance to the crack tip is smaller than in Fig. 3. The plastic zone radius is 4 μm at fracture time.

temperature sensed ahead of the moving crack tip. In fact, the three parameters can be combined to yield a *constant time* parameter according to $t_f + D/v = \text{const.}$, even if each parameter is not determined unambiguously. The nominal parameters of the experiment were $t_f = 56$ μs, $D \cong 1$ mm. The calculated matching velocity is $v = 55$ m/s. If the onset of fracture is assumed to occur at $t_f = 54$ μs, and $D = 2$ mm, the calculated matching velocity is $v = 100$ m/s. In Fig. 5, we have plotted the measured temperature and that calculated for the two sets of parameters. The calculation is stopped at the ultimate time point before the thermocouple is reached by the crack-tip. The ultimate distances for the two sets of parameters are 90 and 10 μm, respectively. These distances lay beyond the plastic zone and are thus acceptable. It must also be noted that the experimental temperature increases past fracture point. This observation, which corresponds to the fact that the crack tip has passed beyond the thermocouple, is not simulated here. Fig. 5 illustrates the relationship between the three parameters, on the one hand, but also essentially the fact that a realistic evolution of the temperature drop is indeed obtained. This result corroborates similar results shown by Rittel (1998b), which were determined directly from the calculated stress intensity factors, using a simple analytical approach. At this stage, it appears that the experimental results are satisfactorily simulated by the numerical model and approach adopted in this work. Therefore additional aspects of the phenomenon can now be explored by "numerical experimentation", as discussed next.

5.4. Angular temperature distribution

Experimental data can be used to predict the temperature distribution around the crack tip. The angular temperature distribution is shown in Fig. 6 for a different (typical) experiment in which fracture was de-

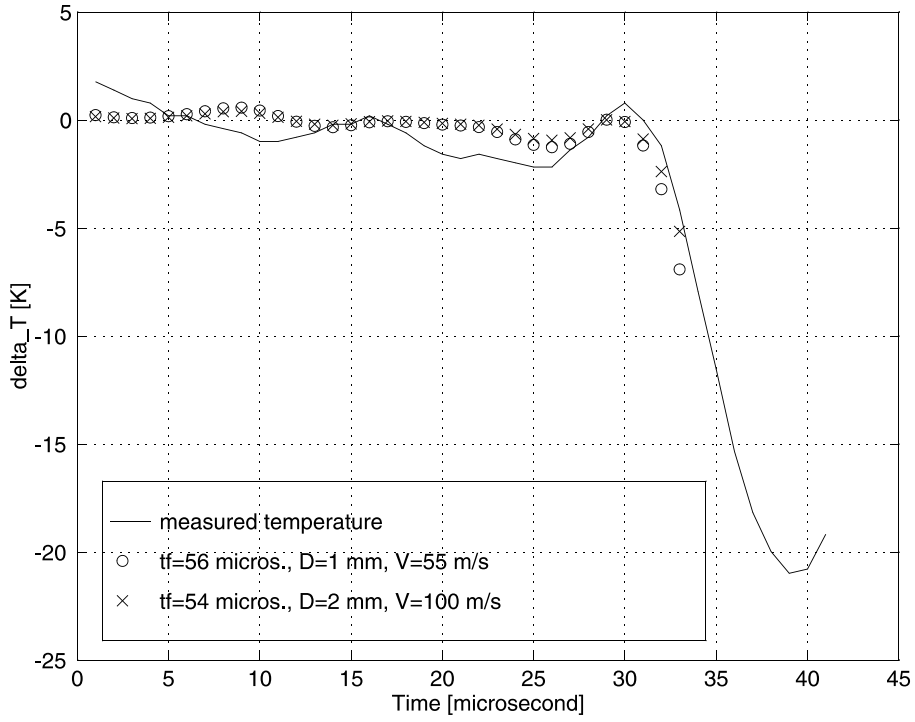

Fig. 5. The measured and numerically simulated temperature drops for the same experiment. The crack is treated as stationary until fracture time, at which it propagates with a constant velocity toward the thermocouple. Two sets of experimental parameters yield the same evolution, which closely follows the actual measurement.

tected at $t_f = 72$ μs. The selected constant radius is 230 μm and four different angles were selected. For this range of angles, the four signals are quite similar. However, the temperature distribution is not symmetric, as shown in Fig. 7 which compares the temperature of two symmetrical points, located 230 μm ahead and behind the crack tip ($\theta = 0°, +0.23$ mm and 180°, -0.23 mm). A slight difference of temperatures (about 2 K) can be noted, as expected from mixed-mode transient loading. While this temperature difference is slight in its absolute value, it is not negligible as it represents about 25% of the temperature drop at fracture.

6. Further numerical results

6.1. Plane strain vs. Plane stress

A simulation of the temperature field was carried out for the two cases of plane stress and plane strain loading of PMMA, with a prescribed gaussian loading (maximal value of 4.10^7 N, 80 μs duration). These results can be used to describe the three-dimensional temperature field, assuming a linear variation of temperature with the thickness. The coordinates system is centered, as before, on the crack tip (r, θ), with the depth, z, being measured from mid-thickness (plane strain). Results are reported in Fig. 8, which shows the evolution of the temperature at two distinct locations ahead of the crack tip as a function of time and thickness. We notice that the temperature drop is smaller under plane stress than under plane strain conditions. The relative temperature variation between mid-thickness and the surface of the

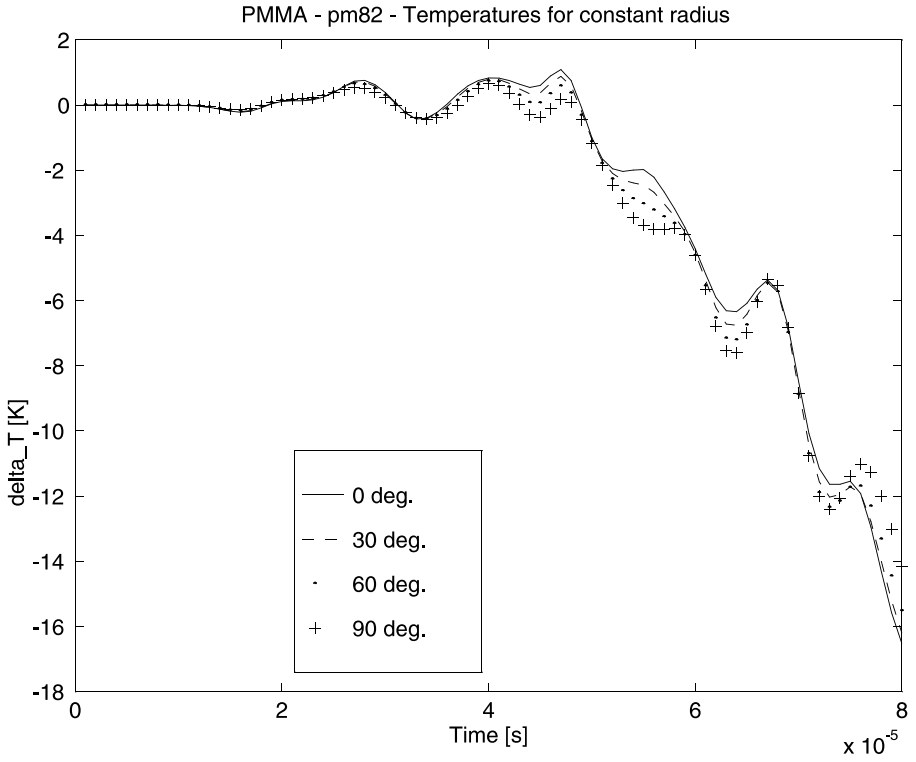

Fig. 6. Calculated angular temperature variation at a constant radius (230 μm) for experimental specimen pm82. Fracture was detected at 72 μs.

specimen is of the order of $\Delta T/T_0 \approx 0.4\%$ ($T_0 = 293$ K). Yet, the *absolute* temperature drop is not negligible under plane stress, even if it is smaller than under plane strain conditions, as expected from LEFM considerations.

6.2. Adiabaticity

Adiabaticity is often assumed to prevail in dynamic fracture because of the short time scales involved (Mason et al., 1994). The validity of this assumption was checked by comparing the results of two identical cases of a PMMA specimen, subjected to the above mentioned gaussian load. In one simulation, the conduction term of the heat equation, $k\nabla^2 T$, was set to zero, to enforce adiabatic conditions (Boley and Weiner, 1960). The results showed *virtually no difference* in the temperature fields calculated in each case, for the investigated duration of 80 μs. This result validates the assumptions of dynamic crack initiation in our (and similar) experiments, for which very short time scales are involved.

6.3. The influence of the thermal conductivity

This simulation was aimed at elucidating the influence of the thermal conductivity on the thermoelastic coupling. Consequently, the calculation was carried out for PMMA ("poor" thermal conductor) and steel ("good" thermal conductor) specimens, whose properties are listed in Table 1. Here too, the above mentioned gaussian was applied, resulting in different stress intensity factors for each material. The stress in-

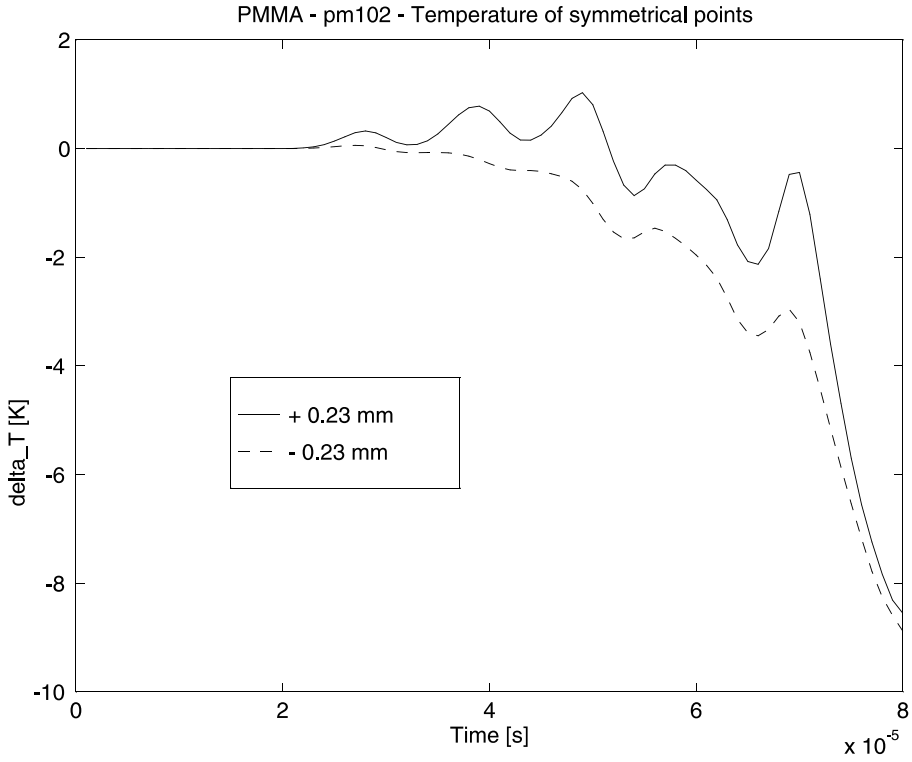

Fig. 7. Calculated temperature variation for experimental specimen pm102 at two symmetric points along the crack line with respect to the tip.

tensity factors have been normalized by the (assumed) mode I dynamic fracture toughness of each material, K_{IC} (5 and 50 MPa $m^{1/2}$). As shown in Fig. 9, mode I is the dominant mode in each case. The wave velocities are higher in steel than in PMMA. As a result, the crack in the steel specimen is loaded at an earlier stage. Fig. 10 shows the temperature drop, at 230 μm ahead of the crack tip, as a function of the absolute (Fig. 10a) and normalized (Fig. 10b) mode I stress intensity factors for each material. From this figure, in which time does not appear explicitly, it appears that PMMA experiences a larger temperature drop than steel for a similar absolute SIF value. However, when the SIF values are normalized with respect to the toughness of the material (Fig. 10b), this trend reverts. At identical normalized stress intensity levels, the steel crack tip experiences a more severe cooling than the PMMA. It should be noted that, despite different plastic zone sizes (of the order of 20 μm for steel and 7 μm for PMMA), the temperatures are calculated in the elastic zone, at a similar distance from the crack-tip. These results show that thermal conductivity is certainly not the single dominant parameter, which determines the amount of crack-tip cooling. Therefore, it is concluded that thermoelastic cooling effects are not restricted to the sole class of low thermal conductivity materials, provided that the elastic response is dominant, as expected (Rittel, 1998a).

7. Summary and conclusions

In this work, we have presented a hybrid experimental–numerical investigation of crack-tip cooling effects in dynamic crack initiation. A simple numerical procedure was devised to treat the conversion of

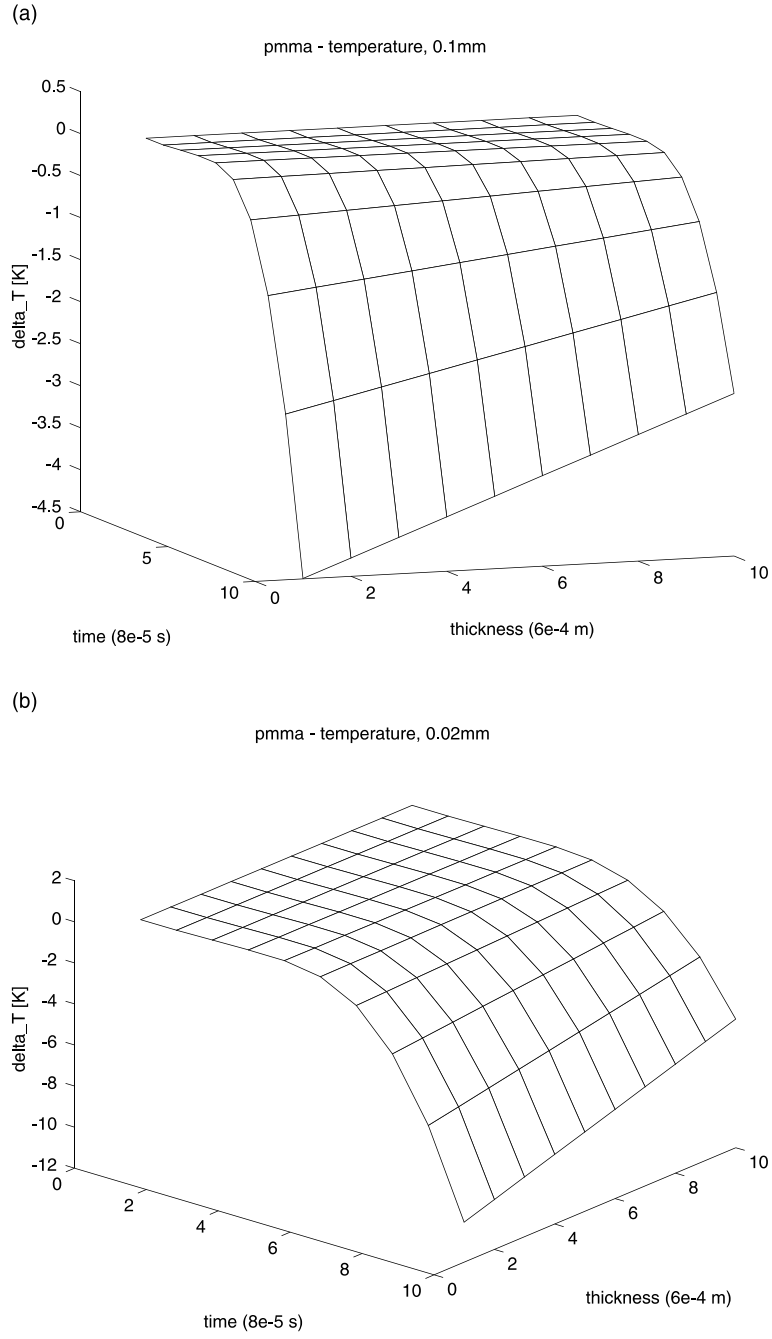

Fig. 8. Numerical experiment: 3D representation of the temperature field. The coordinates origin is centered on the crack-tip at mid-thickness. Note the increased cooling effect at $z = 0$, corresponding to plane strain conditions by contrast with the surface where plane stress conditions prevail. (a) and (b) correspond to 0.1 and 0.02 mm from the crack tip, respectively.

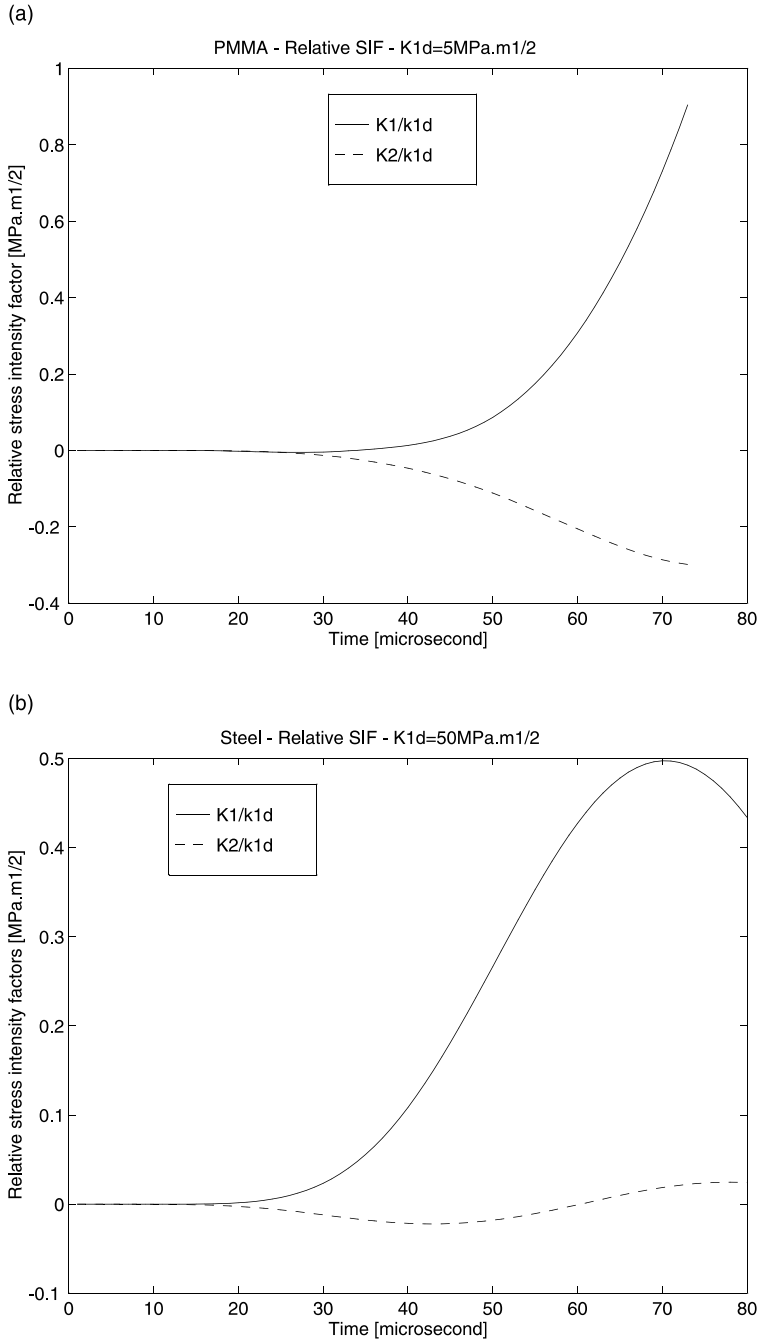

Fig. 9. Numerical experiment: calculated normalized (w/r plane strain fracture toughness) evolutions of the stress intensity factors. (a) PMMA, $K_{IC} = 5$ MPa m$^{1/2}$ and (b) steel $K_{IC} = 50$ MPa m$^{1/2}$.

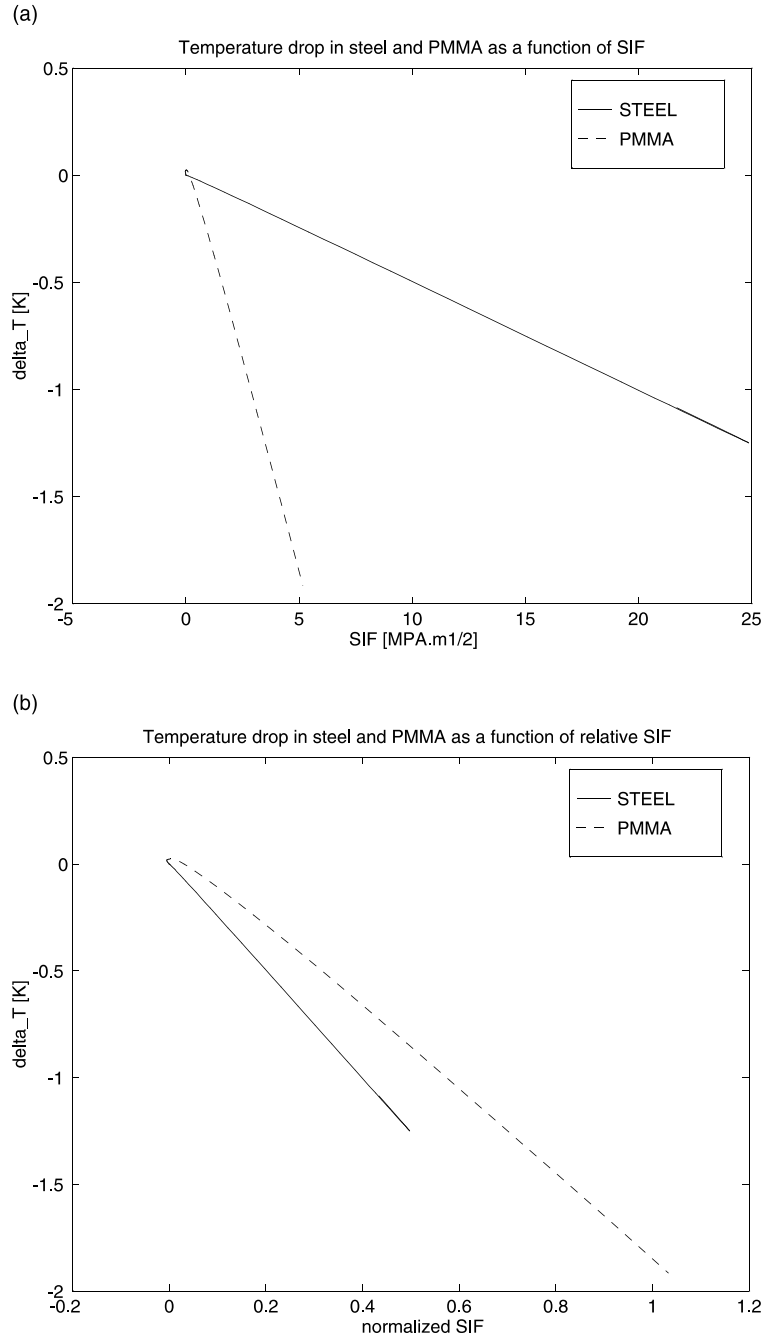

Fig. 10. Numerical experiment: calculated temperature drop for the PMMA and steel specimens, at 230 μm from the crack tip, as a function of (a) absolute SIF: note that PMMA experiences a stronger cooling effect than steel; (b) normalized SIF: the trend is reverted – at identical normalized values of the SIF, steel experiences a slightly larger cooling than PMMA.

mechanical energy into heat for a thermoelastic material, yielding the temperature field around the crack tip. The results of this approach were successfully compared to experimental measurements of the tem-

perature drop in PMMA specimens. Having validated the approach, additional numerical simulations were carried out (numerical experiments). Three issues were addressed: the 3D temperature field, the validity of the assumptions of adiabaticity in dynamic fracture, and the influence of the thermal conductivity on crack-tip cooling.The principal conclusions which can be drawn from this study are as follows:

1. A simple numerical solution was used to calculate the temperature field around the crack tip. The calculated temperatures compare satisfactorily with those measured in experiments.
2. During the transient period, noticeable thermoelastic cooling effects occur.
3. Cooling effects are more pronounced at mid-thickness than on the surface of the specimen.
4. Adiabatic conditions can be reasonably assumed to prevail during dynamic crack initiation.
5. Consequently, cooling effects are expected to prevail during crack initiation in thermoelastic materials, irrespective of their thermal conductivity.

Acknowledgements

Dr. R. Levin's assistance is gratefully acknowledged.

References

ANSYS, User's Manual, 1994. Swanson Analysis Systems Inc.

Barsoum, R.S., 1978. On the use of isoparametric finite elements in linear elastic fracture mechanics. Int. J. Numer. Meth. Engng. 10, 25–37.

Bathe, K.J., 1982. Finite Element Procedures in Engineering Analysis. Prentice Hall, Englewood Cliff, NJ.

Boley, B.A., Weiner, J.H., 1960. Theory of Thermal Stresses. Wiley, New York.

Brock, L.M., 1996. Effects of thermoelasticity and a Von Mises condition in rapid steady-state quasi-brittle fracture. Int. J. Solid. Struct. 33 (28), 4131–4142.

Brock, L.M., 1999a. Rapid crack growth in a thermoelastic solid under mixed-mode thermomechanical loading. IMA J. Appl. Math. 62, 31–44.

Brock, L.M., 1999b. Personal Communication.

Bui, H.D., Maigre, H., Rittel, D., 1992. A new approach to the experimental determination of the dynamic stress intensity factor. Int. J. Solid. Struct. 29 (23), 2881–2895.

Fuller, K.N.G., Fox, P.G., Field, J.E., 1975. The temperature rise at the tip of a fast-moving crack in glassy polymers. Proc. R. Soc. A 341, 537–557.

Holman, J.P., 1986. Heat transfer, sixth ed. McGraw-Hill, Kogakusha.

Maigre, H., Rittel, D., 1993. Mixed-mode quantification for dynamic fracture initiation: application to the compact compression specimen. Int. J. Solid. Struct. 30 (23), 3233–3244.

Maigre, H., Rittel D, 1996. Dynamic fracture detection using the force-displacement reciprocity: application to the compact compression specimen. Int. J. Fracture 73 (1), 67–79.

Mason, J.J., Rosakis, A.J., Ravichandran, G., 1994. On the strain and strain rate dependence of the fraction of plastic work converted into heat: an experimental study using high speed infrared detectors and the Kolsky bar. Mech. Mater. 17, 135–145.

Rabin, Y., Rittel, D., 1999. A model for the time response of solid-embedded thermocouples. Exp. Mech. 39 (1), 132–136.

Rittel, D., 1998a. Experimental investigation of dynamic failure mode transitions. In: Durban, D., Pearson, J.R.A. (Eds.), IUTAM Symposium on Non-linear Singularities in Deformation and Flow. Kluwer Academic Publishers, Dordrecht, pp. 181–192.

Rittel, D., 1998b. Experimental investigation of transient thermoelastic effects in dynamic fracture. Int. J. Solid. Struct. 35 (22), 2959–2973.

Rittel, D., 1998c. Transient temperature measurement using embedded thermocouples. Exp. Mech. 38 (2), 73–79.

Rittel, D., Maigre, H., Bui, H.D., 1992. A new method for dynamic fracture toughness testing. Scripta Metallurgica et Materialia 26, 1593–1598.

Rittel, D., Maigre, H., 1996. An investigation of dynamic crack initiation in PMMA. Mech. Mater. 28, 229–239.

Sih, G.C., Tzou, D.Y., 1986. Heating preceded by cooling ahead of crack: macrodamage free zone. Theor. Appl. Fract. Mech. 6, 103–111.
Sun, N.S., Hsu, T.R., 1996. Thermomechanical coupling effects on fractured solids. Int. J. Fracture 78, 67–87.
Tadmor, Z., 1979. Principles of polymer processing. Wiley, New York.
Weichert, R., Schönert, K., 1978. Heat generation at the tip of a moving crack. J. Mech. Phys. Solid. 26, 151–161.